CONTROL ENGINEERING PRACTICE

Multiphase Rotor Current Observers for Current Predictive Control: a Five-Phase Case Study

Cristina Martín[a,*], Manuel R. Arahal[b], Federico Barrero[a], Mario J. Durán[c]

[a] *Dpto. Ing. Electrónica, Universidad de Sevilla, Spain*
[b] *Dpto. Ing. de Sistemas y Automática, Universidad de Sevilla, Spain*
[c] *Dpto. Ing. Eléctrica, Universidad de Málaga, Spain*

Abstract

The use of multiphase drives has gained importance in recent times due to some advantages that they provide over conventional three-phase ones. High performance stator current control can be achieved by means of direct command of voltage source inverter. In this context finite-state model predictive control is a very flexible strategy that has been recently proposed and analyzed. Nevertheless, its implementation must solve the problem of estimating rotor quantities, being the conventional solution a simple backtracking procedure. In this respect, observers appear as an attractive alternative. However, while they have been used with FOC, sensorless drives and for fault detection, they have not been used yet for predictive control of drives as a way to provide rotor values estimates. In this paper the authors propose to incorporate a full-order rotor current observer in a finite-state model predictive controller of a five-phase induction machine. Pole placement design based on Butterworth filters is used. The new estimation scheme and the standard procedure are compared. By means of experimental tests, the differences between both approaches and the benefits of including a rotor observer are illustrated and verified.

Keywords: Multiphase drives, predictive control, finite-state controller, observer, pole placement.

1. Introduction

In the last decade, research on multiphase electrical machines area has increased due to some specific advantages that they present over the conventional three-phase machines: less current harmonic content, higher overall system reliability, better power distribution per phase and better fault tolerance (Levi, 2008; Levi et al., 2007). Among these machines, asymmetrical six-phase and five-phase induction machines (IM) with sinusoidally distributed stator windings are the most analyzed and proposed in recent works.

Current control strategies in multiphase drives are usually based on a multidimensional extension of common three-phase current controllers, dealing with the difficulties of large harmonic current, unbalanced currents and machine asymmetries (Che et al., 2014; Jones et al., 2009; Yepes et al., 2015). However, these difficulties can be easily overcome eliminating the PWM and commanding the voltage source inverter (VSI) directly by means of model-based predictive control (MPC). Although MPC is a well-established control technique for electrical systems (Chai et al., 2013; Holtz and Stadtfeld, 1983; Lopez et al., 2015; Wang et al., 2014), its application to multiphase IM has increased well after the publication of Levi (2008). Particularly, a new MPC configuration was proposed in Holmes and Martin (1996) in order to eliminate the classical PWM method, giving birth to a control structure that was later named as finite-state MPC (FSMPC) used in multi-phase IM for the first time in Arahal et al. (2009). Since the number of available converter switching states is a finite set, this control structure is also known as finite control set MPC (Choi and Lee, 2015; Rodriguez et al., 2013; Xie et al., 2015). Whatever the denomination, the fast control derived from direct command of the VSI combined with robustness and fault tolerant features that characterize multiphase drives have been analyzed in a number of recent papers (Arashloo et al., 2015; Guzman et al., 2016; Lim et al., 2014; Martinez et al., 2015; Riveros et al., 2013).

A problem encountered in the implementation of FSMPC is the estimation of non-measurable state components; for instance rotor quantities for which sensors are not available. A good knowledge of such quantities is often required in order to provide high performance control. Concerning this, observer theory (Luenberger, 1971) is a well known discipline that provides a framework for understanding and designing estimation schemes and it has been used in electrical systems such as IM drives. Basically, observers used in IM machines can take two forms, a full-order one that permits estimation of stator and rotor components from measurements of stator voltages, sta-

*Corresponding author
Email addresses: cmartin15@us.es (Cristina Martín), arahal@us.es (Manuel R. Arahal), fbarrero@us.es (Federico Barrero), mjduran@uma.es (Mario J. Durán)

http://dx.doi.org/10.1016/j.conengprac.2016.01.011

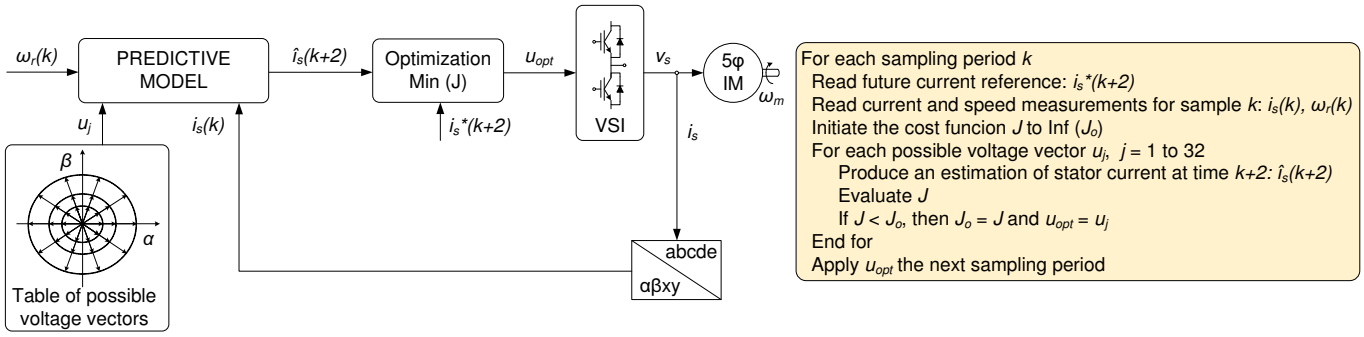

Figure 1: General scheme of the FSMPC method applied to a symmetrical five-phase IM drive (left), and control algorithm (right).

tor currents and speed (Jansen and Lorenz, 1994), and a reduced-order form which provides just the rotor components estimation using only measurements of stator currents and speed.

Most proposals of observers for IM have been made with field oriented control (FOC) method and related ones (El Fadili et al., 2014), even though FOC has been found in practice to be satisfactorily robust and effective without complex flux estimation structures. By contrast, FSMPC is highly sensitive to prediction errors (Arahal et al., 2013) that are caused by parameter mismatch among other reasons (Bogado et al., 2013). In Alireza Davari et al. (2012) sliding mode full-order and reduced-order observers are applied for flux and speed estimation for predictive torque control of IM. A robust model predictive current controller with a disturbance observer is also presented in Xia et al. (2012), where a Luenberger observer is constructed for parameter mismatch and model uncertainty which affects the performance of the MPC. The gains of the disturbance observer are also determined using a root-locus analysis, and the stability of the disturbance observer is analyzed when there are errors in the inductor filter parameter. In Merabet et al. (2006), a nonlinear predictive control law with a disturbance observer is applied to track speed and flux profiles in an IM, considering the robustness to parameters variations and the disturbance rejection. This is in contrast to most applications of FSMPC to electrical systems, where observers are not used as such. Instead nonmeasurable quantities, disturbances and parametric and non-parametric uncertainties are lumped into one single term of the predictive model. This term is then updated using a simple procedure and the update is held until the next sampling period (Arahal et al., 2009).

In this paper a rotor current observer is included in the conventional FSMPC structure. The advantages of this new estimation scheme over the original one are analyzed and experimentally illustrated. For this purpose, a five-phase IM drive is used as a case study. However, the control method can be extended to any n-phase IM drive. Two observers, full-order and reduced-order, are studied. The observer design is tackled using pole placement methodology based on Butterworth filters. The rest of the paper is organized as follows. The general principles of the FSMPC technique and its application to the considered case study system are presented in the next section, where the standard rotor quantities estimation is reviewed and analyzed. The rotor current observers, full-order and reduced-order, are presented in Section 3 together with the design procedure. Experimental results comparing the different estimation methods are shown and discussed in Section 4. The paper ends with the conclusion section.

2. Finite-state model predictive control in five-phase IM drives

The FSMPC application to stator current control in a five-phase drive is schematically illustrated in Fig. 1. The objective of the controller is to track the reference stator currents represented by i_s^*. For this purpose, a discrete model of the physical system is used to predict the future behavior of the output variables $\hat{i}_s$. The prediction is computed making use of measured values of the rotor speed ω_r and the stator phase currents i_s and tentative value of the control vector u_j (the VSI gating signal). The most adequate control action u_{opt} is selected by minimizing a cost function J by means of exhaustive search over all possible control signal values. The optimum gating signal is applied to the VSI during the next sampling period. Finally, this process is repeated every sampling period. More details can be found in Arahal et al. (2009).

2.1. IM drive model

A symmetrical five-phase induction machine with distributed windings equally displaced $\vartheta = 2\pi/5$ and fed by a five-phase two-level VSI is used for testing the proposed method. An approximate scheme of the five-phase IM is shown in Fig. 2, where the gating signals of the VSI are represented by $(K_a, \ldots, K_e)$ and their complementary values $(\bar{K}_a, \ldots, \bar{K}_e)$.

The drive modeling process is made using some standard assumptions: uniform air gap, symmetrical distributed windings, sinusoidal MMF distribution, and negligible core losses and magnetic saturation. The sinusoidal MMF distribution is a well-known assumption in conventional and multiphase induction machines' modelling, provided that

a distributed-winding induction machine is used, as it is discussed in Barrero and Duran (2016); Duran and Barrero (2016); Levi et al. (2007). Then, from the five-phase machine equations in phase variables and following the vector space decomposition (VSD) approach the machine modeling can be represented in two orthogonal subspaces (Levi et al., 2007). One of them, the $\alpha-\beta$ subspace, is involved in the fundamental flux and the torque production, representing the fundamental supply component plus supply harmonics of the order $10n \pm 1$ with $n = 0, 1, 2, 3, ...$ The other, the $x-y$ subspace, is related to the losses and represents supply harmonics of the order $10n \pm 3$. Additionally, a zero sequence harmonic component of the order $5n$ with $n = 1, 2, 3, ...$ is projected in the z-axis, but it is not considered because the neutral point is isolated and consequently zero sequence currents cannot flow. Selecting the $\alpha-\beta$ and $x-y$ stator currents and the $\alpha-\beta$ rotor currents as state variables $x = (i_{s\alpha},\, i_{s\beta},\, i_{sx},\, i_{sy},\, i_{r\alpha},\, i_{r\beta})^T$, the drive equations can be cast in the form

$$\dot{x}(t) = A(\omega_r(t))x(t) + Bv(t)$$

$$y(t) = Cx(t) \tag{1}$$

The input signals are the applied stator voltages $v = (v_{s\alpha},\, v_{s\beta},\, v_{sx},\, v_{sy})^T$, the output signals are the stator currents $y = (i_{s\alpha},\, i_{s\beta},\, i_{sx},\, i_{sy})^T$ and the matrices A and B depend on the rotor electric speed ω_r and the following machine parameters, stator and rotor resistances R_s and R_r, stator and rotor inductances L_s and L_r, stator leakage inductance L_{ls} and mutual inductance M.

$$A(\omega_r) = \begin{pmatrix} -a_{s2} & a_{m4}(\omega_r) & 0 & 0 & a_{r4} & a_{l4}(\omega_r) \\ -a_{m4}(\omega_r) & -a_{s2} & 0 & 0 & -a_{l4}(\omega_r) & a_{r4} \\ 0 & 0 & -a_{s3} & 0 & 0 & 0 \\ 0 & 0 & 0 & -a_{s3} & 0 & 0 \\ a_{s4} & -a_{m5}(\omega_r) & 0 & 0 & -a_{r5} & -a_{l5}(\omega_r) \\ a_{m5}(\omega_r) & a_{s4} & 0 & 0 & a_{l5}(\omega_r) & -a_{r5} \end{pmatrix} \tag{2}$$

$$B = \begin{pmatrix} c_2 & 0 & 0 & 0 \\ 0 & c_2 & 0 & 0 \\ 0 & 0 & c_3 & 0 \\ 0 & 0 & 0 & c_3 \\ -c_4 & 0 & 0 & 0 \\ 0 & -c_4 & 0 & 0 \end{pmatrix} \tag{3}$$

The above matrices coefficients are given by $c_1 = L_s L_r - M^2$, $c_2 = L_r/c_1$, $c_3 = 1/L_{ls}$, $c_4 = M/c_1$, $c_5 = L_s c_1$, $a_{s2} = R_s c_2$, $a_{s3} = R_s c_3$, $a_{s4} = R_s c_4$, $a_{r4} = R_r c_4$, $a_{r5} = R_r c_5$, $a_{l4}(\omega_r) = L_r c_4 \omega_r$, $a_{l5}(\omega_r) = L_r c_5 \omega_r$, $a_{m4}(\omega_r) = M c_4 \omega_r$ and $a_{m5}(\omega_r) = M c_5 \omega_r$.

The predictive model must also include the VSI dynamic, since it forms part of the IM drive. An ideal inverter converts gating signals into stator voltages that can be projected to $\alpha-\beta-x-y$ axes and gathered in a row vector computed as $v = (v_{s\alpha},\, v_{s\beta},\, v_{sx},\, v_{sy}) = V_{dc} u T M$,

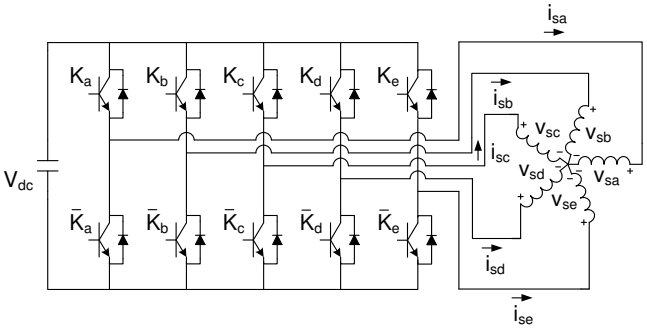

Figure 2: Five-phase IM drive schematic diagram.

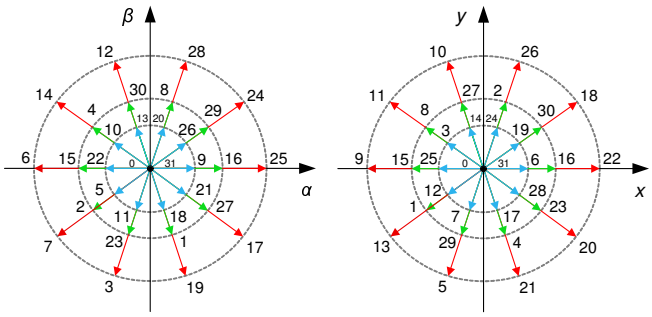

Figure 3: Space vector diagrams in the $\alpha-\beta$ and $x-y$ subspaces.

where V_{dc} is the DC-link voltage, u is a row vector containing the gating signals, T is the connectivity matrix that takes into account how the VSI gating signals are distributed and M is a coordinate transformation matrix accounting for the spatial distribution of the machine windings:

$$T = \frac{1}{5}\begin{pmatrix} 4 & -1 & -1 & -1 & -1 \\ -1 & 4 & -1 & -1 & -1 \\ -1 & -1 & 4 & -1 & -1 \\ -1 & -1 & -1 & 4 & -1 \\ -1 & -1 & -1 & -1 & 4 \end{pmatrix} \tag{4}$$

$$M = \frac{2}{5}\begin{pmatrix} 1 & \cos\vartheta & \cos 2\vartheta & \cos 3\vartheta & \cos 4\vartheta \\ 0 & \sin\vartheta & \sin 2\vartheta & \sin 3\vartheta & \sin 4\vartheta \\ 1 & \cos 2\vartheta & \cos 4\vartheta & \cos\vartheta & \cos 3\vartheta \\ 0 & \sin 2\vartheta & \sin 4\vartheta & \sin\vartheta & \sin 3\vartheta \\ 1/2 & 1/2 & 1/2 & 1/2 & 1/2 \end{pmatrix} \tag{5}$$

In the case of a 5-legged inverter, the gating signals vector is defined as $u = (K_a,\, K_b, ...,\, K_e)$ where K_j is the j-th gating signal. Since each gating signal can be either active $K_j = 1$ or inactive $K_j = 0$, there exist 2^5 possible control choices and voltage vectors. Fig. 3 shows all possible voltage vectors where each one is identified using the decimal number corresponding to the binary code of the switching state.

Eqs. (1)-(3) together with the inverter model define the final drive model as a nonlinear set of equations. These equations must be discretized in order to be used for the predictive controller. A forward Euler method is usually

used, leading to the following expression that constitutes the predictive model:

$$\hat{x}(k+1|k) = x(k) + T_s\left(A(\omega_r(k))x(k) + Bv(k)\right) \quad (6)$$

denoted by T_s the sampling time, k the current sample time and $\hat{x}(k+1|k)$ the one-step ahead prediction of the system state computed at current time k. Notice that matrix A depends on the instantaneous value of the rotor electric speed, thus the predictive model is a time-variant linear system. However, the mechanical speed dynamics are slower than the electrical dynamics, so constant speed within a sampling period can usually be assumed.

2.2. State estimation

The predictive model (6) presented in the previous section cannot be used as such in a typical configuration in which rotor currents are not measured. This difficulty is conventionally overcome lumping all non-measurable terms into one factor, constituting a new variable that is estimated using past values of the measured variables. The estimated term is then projected into the future and used in the predictive model, being updated every sampling period. In the present case, it is necessary to split the state vector into a measurable part $x^1 = (i_{s\alpha},\, i_{s\beta},\, i_{sx},\, i_{sy})^T$ and an unmeasurable part $x^2 = (i_{r\alpha},\, i_{r\beta})^T$. Thus, the prediction is obtained by simulating for a sampling period the evolution of the measurable part as

$$\hat{x}^1(k+1|k) = Rx^1(k) + Sv(k) + \hat{G}(k|k) \quad (7)$$

where

$$R = (I + A_{11}T_s) \quad (8)$$

$$S = B_1 T_s \quad (9)$$

and term $\hat{G}(k|k)$ is an estimation of the contribution of $x^2(k)$ to $x^1(k+1)$. It is usually obtained by holding its previous value $\hat{G}(k-1)$ computed at time k as

$$\hat{G}(k-1|k) = x^1(k) - Rx^1(k-1) - Sv(k-1) \quad (10)$$

The computation of the control signal takes a significant amount of time, being comparable with the sampling time. Consequently, it is desirable to wait until the next sampling time to release the computed control signal (more details in Arahal et al. (2009)). Taking this into account, a second-step ahead prediction has to be computed, being the current prediction at time $k+2$ obtained at time k as

$$\hat{x}^1(k+2|k) = Rx^1(k+1|k) + Sv(k) + \hat{G}(k|k) \quad (11)$$

In stator current control in multiphase IM, the cost function should incorporate the predicted deviations from current references in the $\alpha-\beta$ and $x-y$ subspaces in the following way:

$$J = \|\hat{e}_{\alpha\beta}\|^2 + \lambda_{xy}\|\hat{e}_{xy}\|^2 \quad (12)$$

where $\hat{e}$ is the second-step ahead predicted error $\hat{e} = i_s^*(k+2) - \hat{i}_s(k+2|k)$ and λ_{xy} is a tuning parameter that allows more emphasis on $\alpha-\beta$ or $x-y$ subspaces. More complicated cost functions can be devised in order to include other aspects to be optimized, such as harmonic content and VSI losses.

2.3. Analysis of the simple update and hold method

To the best of our knowledge, the backtracking procedure introduced in the previous section has not been analyzed in the literature yet, and thus the following study is novel and relevant as most proposed FSMPC applications rely on said procedure.

As already stated, the usual way to cope with unmeasurable quantities in FSMPC is to lump them into one term that is estimated in a simple manner. The term is designated as G and used in the first-step ahead prediction as

$$\hat{x}^1(k+1|k) = Rx_m^1(k) + Sv(k) + \hat{G}(k|k) \quad (13)$$

Ideally the term $G(k-1)$ could be computed at time k by means of

$$G(k-1) = x^1(k) - Rx^1(k-1) - Sv(k-1) \quad (14)$$

but, due to measurement errors ε, the actual estimation is

$$\hat{G}(k-1|k) = x_m^1(k) - Rx_m^1(k-1) - Sv(k-1) \quad (15)$$

where $x_m^1(k)$ is the measured vector of stator quantities, linked to the real values through

$$x_m^1(k) = x^1(k) + \varepsilon(k) \quad (16)$$

Making use of the state-space equations the estimation can be written as

$$\hat{G}(k-1|k) = \varepsilon(k) - R\varepsilon(k)(k-1) + A_{12}T_s x^2(k-1) \quad (17)$$

From this equality it is inferred that the estimation of rotor quantities done in this way is corrupted by the measurement error. The error of the first step ahead prediction is defined as

$$e_{1p}(k+1) \doteq x^1(k+1) - \hat{x}^1(k+1|k) \quad (18)$$

and can be computed from previous expressions as

$$\begin{aligned} e_{1p}(k+1) = {} & Rx^1(k) + Sv(k) + G(k) - \\ & - \left(Rx_m^1(k) + Sv(k) + \hat{G}(k-1|k)\right) \end{aligned} \quad (19)$$

It is easy to show that the above equation yields the following expression for the one-step ahead prediction error

$$\begin{aligned} e_{1p}(k+1) = {} & -(I+R)\varepsilon(k) + R\varepsilon(k)(k-1) + \\ & + A_{12}T_s\left(x^2(k) - x^2(k-1)\right) \end{aligned} \quad (20)$$

From (20) one can derive that the prediction error arising from this scheme does not filter measurement errors.

On average, the prediction error due to this factor will exhibit the same statistical properties as ε. Assuming uncorrelated error measurement with a distribution with zero mean and σ^2 variance, the contribution to e_{1p} variance is precisely σ^2. However the instantaneous contribution can be large, for instance if $\varepsilon(k) = -\varepsilon(k-1) = n$ then $-(I + R)\varepsilon(k) + R\varepsilon(k)(k-1) = (I+2R)n = (3I+2A_{11}T_s)n \approx 3n$. Consequently, a small amount of noise can produce large deviations in the estimation of the state. This has a profound impact on the performance of the current control because a wrong voltage vector would be selected producing a disturbance that should be canceled at later sampling times. In Arahal et al. (2013) it is shown that current total harmonic distortion (THD) is greatly influenced by this phenomenon.

Regarding rotor quantities, it is interesting to see that the contribution to the prediction error is filtered through the system dynamic via the term $A_{12}T_s$. For larger sampling frequencies the effect is smaller, which is part of the reason why most applications uses a high value of f_s. Also from the above expression one can see that it is the change in rotor quantities that induces prediction error. In sinusoidal steady state the rotor quantities are expected to evolve, for the most part, at the fundamental frequency f_e. Again, if a large f_s/f_e is used then the changes from one sampling period to the next would be small (ceteris paribus), allowing the standard simple estimation scheme to provide acceptable results. A problem might arise during transients where changes can be more pronounced, or in situations where harmonics are noticeable and fast variations in rotor quantities appear. This is potentially dangerous as harmonics can be triggered by erroneous predictions as indicated in the previous paragraph.

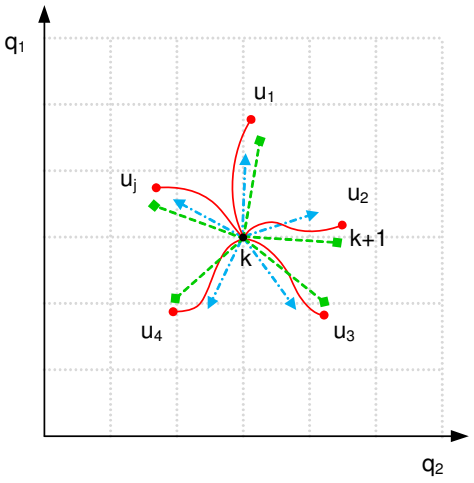

Figure 4: Illustration of conventional and observer-based predictions. Red lines with circle marks (solid) represent the real trajectory after applying a certain voltage vector. Blue lines with triangle marks are predicted trajectories using the simple rotor quantities estimation and green lines with square marks are predicted trajectories using an observer.

Fig. 4 illustrates the effect of using the simple estimation procedure for rotor quantities. The graph is a state-space or phase-portrait diagram, where the q_1 and q_2 axis symbolize the state components. The state at time k (shown as a dot in the middle) can evolve with time, providing different values at $k+1$ depending on the choice of the control action $u(k)$. The standard simple estimation method provides predictions (blue lines) with an error given by (20). It will be shown later that observers can provide more adequate predictions (green lines).

The correctness of the predictions plays a crucial role in FSMPC because control actions are based on them. Note that the large number of available voltage vectors in multiphase VSI and the particularity of the cost function provides a scenario in which mildly incorrect predictions result in the choice of different optimal voltages. This will be illustrated in the experimental results section.

3. Rotor current observer design and implementation

In Fig. 5 the conventional FSMPC technique is presented including an optional observer to estimate the rotor quantities. The rotor current estimation $\hat{i}_r$ is calculated by the observer using the measured rotor speed ω_r and stator phase currents i_s for every sampling time, allowing the complete state-space model (1) to be employed for predictive purposes.

The observer order is defined by the number of system state variables employed in its construction. In the following sections, the design and implementation of two observer configurations with different orders are presented: full-order observer and reduced-order observer.

3.1. Full-order rotor current observer

The basic observer configuration permits an estimation of all system states $\hat{x}(t)$ from the system model, plus a correction term which is proportional to the estimate error

$$\dot{\hat{x}}(t) = A\hat{x}(t) + Bv(t) - L\left(C\hat{x}(t) - y(t)\right) \tag{21}$$

From observer theory, it is known that the closed loop poles of the observer defined in (21) are determined by the observer gain L, also called Luenberger gain matrix. The observer error dynamic equation can be simplified to

$$\dot{e}(t) = \dot{\hat{x}} - \dot{x} = (A - LC)\, e(t) \tag{22}$$

and the convergence towards zero is determined by the choice of the observer gain. The separation principle allows the choice of such matrix to be decoupled from the controller design.

3.2. Reduced-order rotor current observer

The stator current's estimation obtained from the full-order observer leads to a redundancy, since they are already available by direct measurement. This redundancy

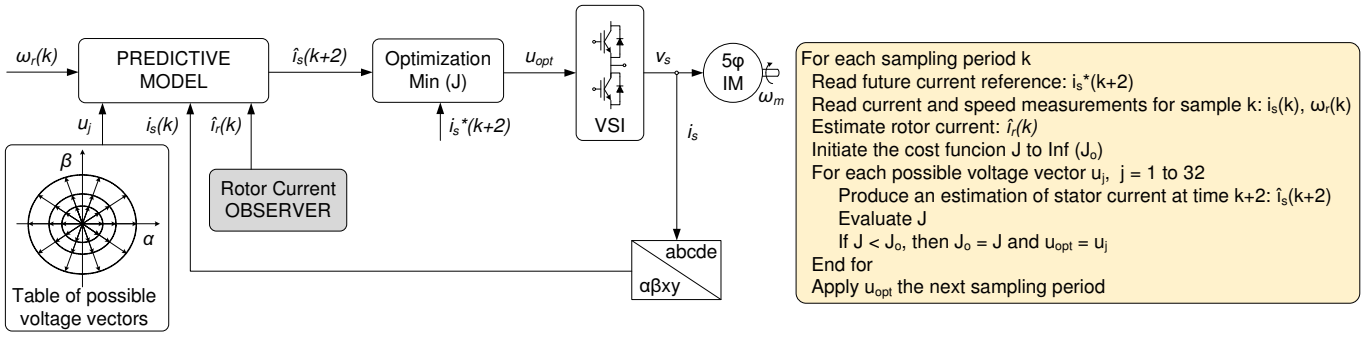

Figure 5: General scheme of the FSMPC with rotor current observer method applied to a symmetrical five-phase IM drive (left), and control algorithm (right).

can be eliminated by constructing an observer of lower dimension that might be useful for reducing the computation time.

A reduced-order observer for i_r can be derived using Gopinath's method (Gopinath, 1971). For the case of study, the system's state is divided in two parts, the measurable one $x^1 = (i_{s\alpha}, i_{s\beta})^\top$ and the unmeasurable one $x^2 = (i_{r\alpha}, i_{r\beta})^\top$. Matrices A and B are accordingly divided so that

$$\begin{aligned} \dot{x}^1(t) &= A_{11}x^1(t) + A_{12}x^2(t) + B_1 v(t) \\ \dot{x}^2(t) &= A_{21}x^1(t) + A_{22}x^2(t) + B_2 v(t) \end{aligned} \tag{23}$$

The estimation for the unmeasurable part is computed in the following way

$$\hat{x}^2(t) = z(t) + Lx^1(t) \tag{24}$$

where the $z(t)$ dynamic is dictated by

$$\begin{aligned} \dot{z}(t) = &\left(A_{22} - LA_{12}\right) z(t) + \left(A_{22} - LA_{12}\right) Lx^1(t) \\ &+ \left(A_{21} - LA_{11}\right) x^1(t) + \left(B_2 - LB_1\right) v(t) \end{aligned} \tag{25}$$

Finally, the reduced-order estimator error is now

$$\dot{e}(t) = \dot{\hat{x}}^2 - \dot{x}^2 = \left(A_{22} - LA_{12}\right) e(t) \tag{26}$$

This observer configuration reduces the computational load required to estimate all state variables when the full-order observer is employed.

3.3. Observer design with Butterworth pole placement

A correct observer design should consider the effect of gain matrix L in all terms of the error dynamic to provide a tradeoff between fast convergence and disturbance sensitivity. Observer theory suggests ad hoc modifications of the estimator that often yield faster convergence without endangering stability (Verghese and Sanders, 1988). Additionally, the poles of classical observers for IM are placed proportionally to the IM poles, which produce high imaginary parts at high speed and deteriorate the system stability. In Zhang and Yang (2014) it is suggested the imaginary part be equal to that of the IM poles and the real part be shifted to the left in the complex plane compared to the original poles. However, this leads to complicated expressions of observer gains. The authors propose a very simple constant gain matrix to improve the stability of the observer.

The design of both full-order and reduced-order observers implies the selection of the most adequate eigenvalues of $(A - LC)$ and $(A_{22} - LA_{12})$, respectively. As they determine the speed at which the estimation error decays, it is logical to make the real parts of those eigenvalues as negative as possible. But this logic does not work well when modeling errors need to be considered. In this regard, research has shown that in order for the observer to be robust against modeling errors, as well as causing the estimation error to decay rapidly, a different approach is required.

It is also of importance that the observer has well-damped dynamics. Good damping of a system implies that the poles are located some distance away from the origin in order to speed-up the convergence and with imaginary parts no larger than the real parts. The latter is desirable in order to avoid oscillatory behavior. With poor damping, there is also a risk for instability if the observer is implemented using forward Euler discretization (Verghese and Sanders, 1988).

Finally, if the original system has z_1 stable zeros, then z_1 of the observer's eigenvalues should keep those positions. The remaining eigenvalues of the observer may be placed into the left-half plane, but at locations that are equidistant from the origin in what is known as the Butterworth configuration. Therefore, a Butterworth polynomial is the equation employed to calculate the eigenvalues. This polynomial represents the denominator of a low-pass filter in the area of signal processing. The step response of such filters has a slight overshoot, with good damping. Consequently, it is desirable to place the poles of the observer in the locations given by the roots of a proper Butterworth polynomial in order to obtain good damping and rising times with respect to the error dynamic.

The full-order observer needs a sixth order Butterworth filter to evaluate its poles. However, the model of the system presents two real poles for the case of study. A

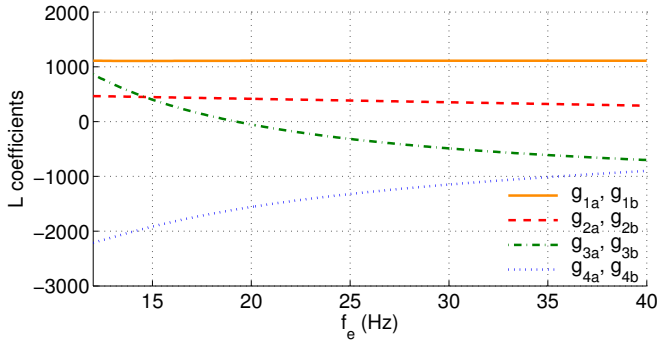

(a)

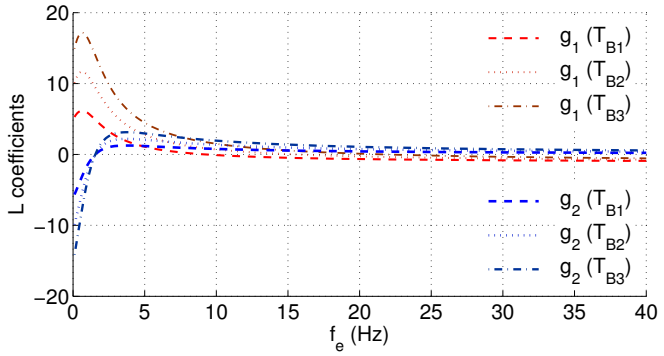

(b)

Figure 6: (a) Variation of L_{FO} coefficients vs f_e. (b) Variation of L_{RO} coefficients vs f_e for some values of T_B.

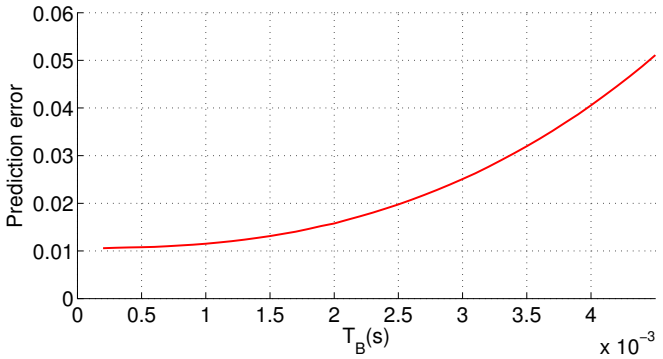

(a)

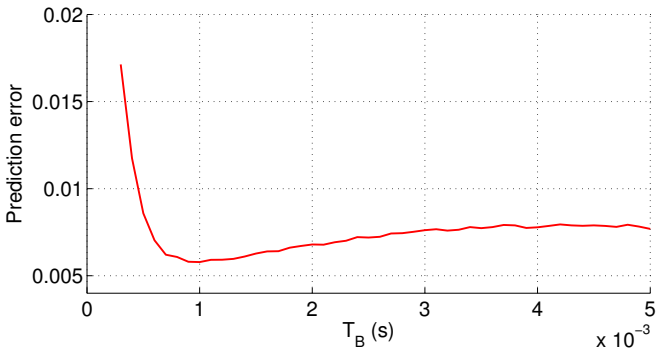

(b)

Figure 7: Prediction error dependence on parameter T_B used to tune (a) the full-order observer and (b) the reduced-order observer.

more proper solution consists of placing four of the observer poles using a fourth order filter and shifting the original two real poles to the left in order to speed up the observer error dynamic. The characteristic polynomial of a fourth order Butterworth filter is

$$B_4(s) = T_B^4 s^4 + 2.6131 T_B^3 s^3 + 3.4142 T_B^2 s^2 + 2.6131 T_B s + 1 \tag{27}$$

where parameter T_B is used to define the speed of the response, with such speed inversely proportional to T_B.

On the other hand, a second order Butterworth filter is necessary to determine the poles of the proposed reduced-order observer. The filter characteristic polynomial is now

$$B_2(s) = T_B^2 s^2 + \sqrt{2} T_B s + 1 \tag{28}$$

Once the desired closed loop observer poles are computed using (27) and (28), Luenberger matrix coefficients are derived using the Kautsky-Nichols algorithm (Kautsky et al., 1985), resulting in the following Luenberger matrices L_{FO} and L_{RO} for the full-order and reduced-order observers, respectively:

$$L_{FO} = \begin{pmatrix} g_{1a} & g_{2a} & 0 & 0 \\ -g_{2b} & g_{1b} & 0 & 0 \\ 0 & 0 & g_5 & 0 \\ 0 & 0 & 0 & g_5 \\ g_{3a} & -g_{4a} & 0 & 0 \\ g_{4b} & g_{3b} & 0 & 0 \end{pmatrix} \tag{29}$$

$$L_{RO} = \begin{pmatrix} g_1 & -g_2 \\ g_2 & g_1 \end{pmatrix} \tag{30}$$

Now, as the coefficients of A and A_{22} are dependent on ω_r, it is necessary to solve the pole placement problem for the current value of ω_r on-line. In order to avoid the required computing load, it is convenient to derive expressions for the elements of the gain matrices as a function of ω_r; or to use a pre-computed set of coefficients and interpolate. In the latter case, the resulting observer is equivalent to a gain scheduled system and its performance depends on the schedule resolution as well as on the accuracy of the measured values of ω_r.

Fig. 6a shows the variation of L_{FO} coefficients with the electrical frequency f_e. Coefficient g_5 has not been represented because its value is constant for all frequencies and T_B. Coefficients' values are almost equal in pairs throughout the frequency range. For that reason, they have been depicted as equal for clarity of representation. Also, the evolution of these parameters can be approximated by simple equations that permit the computation of a new gain matrix on-line, avoiding the Kautsky-Nichols algorithm. However, these coefficients vary with T_B, so different equations have to be defined.

On the other hand, the L_{RO} gain matrix coefficients are shown in Fig. 6b for different frequencies and for $T_{B1} = 0.0025$ s, $T_{B2} = 0.0014$ s, and $T_{B3} = 0.001$ s. It can be seen that the variation in the coefficients' values

is smooth, allowing one to rely on interpolation if a sufficiently high number of discrete samples is given, validating this interpolation for all T_B.

To complete the observer design, an adequate value of T_B must to be chosen. Fig. 7 shows the variation of the prediction error with T_B for both full-order and reduced-order observers. It can be seen in both cases that there is an optimum value of T_B that minimizes the error. The errors have been obtained via extensive simulation using a model of the IM with a FSMPC that makes use of the observer. In the real machine the minimum is obtained for a slightly different value that will be used in the experiments shown in the next section.

3.4. Analysis of the robustness of the observer

Changes in real parameters might cause the observer to use an inaccurate model. In the following a new derivation of the state estimation error is made taking into account this possibility. In the general case, the complete system model has the form

$$\dot{x} = Ax + Bu + Dd$$
$$y = Cx + Hd \tag{31}$$

If perfect knowledge of the parameters cannot be achieved then the observer model uses a different set of matrices

$$\dot{\hat{x}} = A_o\hat{x} + B_o u + K\left(C_o\hat{x} - y\right) \tag{32}$$

where x is the state vector of the system; u is the measurable, or otherwise known, inputs to the systems; d is the unmeasurable term representing external disturbances acting on the system (in most cases structural and parametric uncertainty are lumped into this term); y is the measurable output vector; A, B, C, D, H are matrices containing the coefficients of the state space representation; A_o, B_o, C_o are matrices containing the coefficients of the state space representation used by the observer; and K is the observer gain or Luenberger gain matrix. In this particular case $C_o = C$ as there is no uncertainty about which state variable is considered the output.

The state estimation error, defined as $\xi = \hat{x} - x$, is a dynamical variable that evolves from an initial condition given by the choice of $x(0)$. In most cases found in the literature, a good agreement is supposed between observer and system models and thus the error dynamics equation is simplified to (22). However, if the effect of parameter uncertainty is considered then the estimation error dynamics are given by

$$\dot{\xi} = \left(A_o + KC_o\right)\hat{x} - \left(A + KC\right)x + \left(B_o - B\right)u - \left(D + KH\right)d \tag{33}$$

By algebraic manipulation and after some renaming of terms, the above equation can be written as

$$\dot{\xi} = P_o\xi - \left(A - A_o\right)x + Qu - Zd \tag{34}$$

where $P_o = A_o + KC_o$, $Q = B_o - B$ and $Z = D + KH$. Lumping the last three terms into one variable $W = -\left(A - A_o\right)x + Qu - Zd$ one gets

$$\dot{\xi} = P_o\xi + W \tag{35}$$

Note that the state estimation error converges to zero thanks to the appropriate choice of K because the term W is bounded (as follows from the fact that x, u and d are bounded signals). This convergence of the estimated state to the real value ensures that the effect of parameter uncertainty appears only in the prediction phase, where matrices A_o and B_o are used again. This is in contrast with standard FSMPC where both the state estimation and the resulting predictions are subject to inaccuracies arising from parametric uncertainty.

4. Experimental results for the case of study

A laboratory experimental setup (depicted in Fig. 8) has been designed to compare the performance of FSMPC with different rotor quantities estimation procedures. The main component is a 30-slot five-phase induction machine with three pairs of poles, whose parameters have been obtained experimentally using assumptions and methods described in Yepes et al. (2012) and Riveros et al. (2012) and are summarized in Table 1. Notice that the leakage inductance in $x-y$ plane is considered equal to the leakage inductance in $\alpha - \beta$ plane, since the five-phase induction machine is single-layer (Hadiouche et al., 2004). The IM is fed by means of two SKS21F three-phase inverters from Semikron, which are connected to a DC-link voltage of 300V using an independent DC power supply. The control algorithm is deployed in a TM320F28335 DSP placed on a MSK28335 Technosoft board. A variable load can be introduced in the system thanks to a DC motor attached directly to the shaft of the induction machine. Finally, for the purpose of measuring the mechanical rotor speed a GHM510296R/2500 digital encoder is used together with the enhanced quadrature encoder pulse (eQEP) peripheral of the DSP.

Several experiments have been carried out to provide data for comparison of three controllers: FSMPC employing the conventional backtracking procedure, FSMPC with a reduced-order rotor current observer or RLO from now

Table 1: Electrical and mechanical parameters of the five-phase IM

Parameter		**Value**
Stator resistance	$R_s(\Omega)$	19.45
Rotor resistance	$R_r(\Omega)$	6.77
Stator leakage inductance	L_{ls}(mH)	100.7
Rotor leakage inductance	L_{lr}(mH)	38.6
Mutual inductance	M(mH)	656.5
Mechanical nominal speed	ω_n(rpm)	1000
Power	P(kW)	1
Pairs of poles	p	3

on, and FSMPC with full-order rotor current observer or FLO. The steady-state response of the machine, which operates in torque mode, has been analyzed in each experiment for different stator current references i_s^* defined by a frequency f_e and an amplitude A_{ref}. This allows the characterization of the stator current control under different operation points and the comparison of the three controllers in a high range of operating conditions.

All tests are realized using a sampling frequency of $f_s = 15$ kHz (sampling time $T_s = 66.67\mu$s), a cost function tuning parameter of $\lambda_{xy} = 0.1$ and a load torque of 58% of the nominal one. The observers are implemented using the Butterworth pole placement method previously introduced with $T_B = 1/1000$ s for the full-order observer and $T_B = 1/1300$ s for the reduced-order observer. These are experimental values close to the theoretical ones found in Fig. 7, but they produce better results.

The experimental results and conditions are depicted in Table 2. The type of controller used in each experiment can be seen in the first column. The two following columns indicate the electrical frequency and amplitude of the stator current reference. The next three columns detail the root-mean-squared (RMS) error in the current tracking for the α component e_α^{RMS} and for the $x-y$ components e_{xy}^{RMS}, and the RMS error of the two-step ahead prediction in the α current component $\hat{e}_\alpha^{RMS}$. These quantities are computed as follows:

$$e_\alpha^{RMS} = \sqrt{\frac{\sum_{j=1}^{N}(i_{s\alpha}(j) - i_{s\alpha}^*(j))^2}{N}} \tag{36}$$

$$e_{xy}^{RMS} = \sqrt{\frac{\sum_{j=1}^{N}(i_{sx}(j)^2 + i_{sy}(j)^2)}{N}} \tag{37}$$

$$\hat{e}_\alpha^{RMS} = \sqrt{\frac{\sum_{j=1}^{N}(\hat{i}_{s\alpha}(j+2) - i_{s\alpha}(j+2))^2}{N}} \tag{38}$$

The last two columns in Table 2 present the total harmonic distortion THD and the number of switching changes per cycle N_c for each test. The first one is calculated as the average value of the total harmonic distortion in the α and β components of the stator current

$$THD_{\alpha\beta} = \sqrt{\frac{\int_0^\infty (i_{s\alpha\beta}(t) - i_{s\alpha\beta 1}(t))^2 dt}{\int_0^\infty (i_{s\alpha\beta 1}(t))^2 dt}} \tag{39}$$

where $i_{s\alpha\beta 1}$ is the fundamental component in the α and β axes of the measured current. The N_c parameter is obtained as the average value of the number of switch changes per cycle (SCPC).

It can be easily stated from the results that the use of a rotor observer improves the performance of the current controlled system, considerably reducing the tracking errors and the others considered figures of merit. What is more, this improvement is higher when the full-order observer is employed. To support the results shown in Table 2, the experimental results for one of the operation points

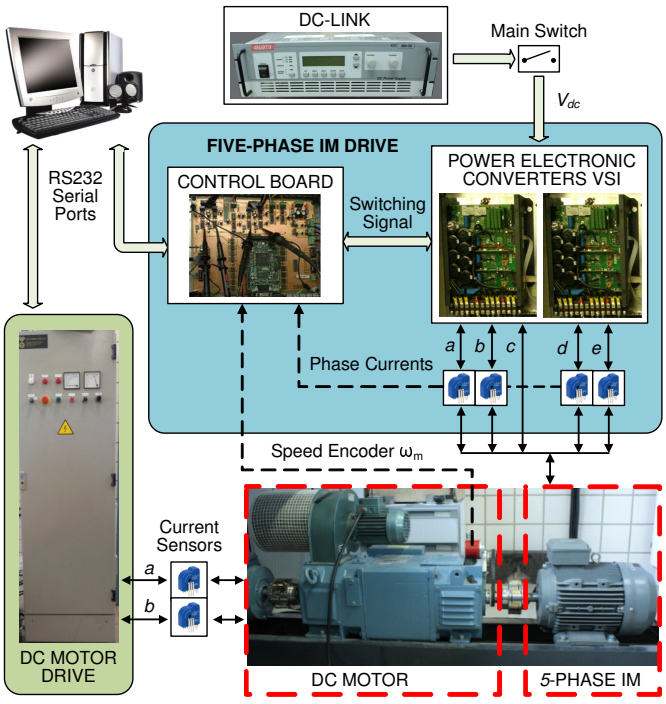

Figure 8: Experimental test rig diagram showing two conventional three-phase VSIs (upper right), the electronic control board (center middle), the DC motor drive (left side), and the IM machine and the DC motor (bottom right).

Table 2: Experimental results for different controllers and references

Ctrl.	e_α^{RMS} (x10^{-2})	e_{xy}^{RMS} (x10^{-2})	$\hat{e}_\alpha^{RMS}$ (x10^{-2})	THD (%)	N_c (SCPC)
$f_e = 19$ Hz, $A_{ref} = 1.47$ A					
FSMPC	10.71	17.74	14.38	10.15	141.03
RLO	8.93	13.36	10.30	10.36	115.11
FLO	7.32	8.85	7.80	8.56	112.45
$f_e = 24$ Hz, $A_{ref} = 1.50$ A					
FSMPC	10.96	17.75	14.25	8.69	96.97
RLO	8.36	13.09	10.17	7.95	83.23
FLO	7.12	8.41	8.34	6.46	72.06
$f_e = 29$ Hz, $A_{ref} = 1.62$ A					
FSMPC	10.91	18.44	15.07	7.09	68.10
RLO	7.84	14.34	10.31	6.96	56.87
FLO	6.61	8.28	8.93	5.22	51.25
$f_e = 34$ Hz, $A_{ref} = 1.56$ A					
FSMPC	11.23	18.89	15.41	7.24	50.56
RLO	7.82	15.38	10.42	6.63	39.20
FLO	6.12	8.27	9.27	5.10	39.03
$f_e = 39$ Hz, $A_{ref} = 1.60$ A					
FSMPC	12.12	21.76	16.02	6.39	35.30
RLO	7.82	18.17	10.68	5.70	25.83
FLO	6.10	12.74	10.40	4.46	23.24

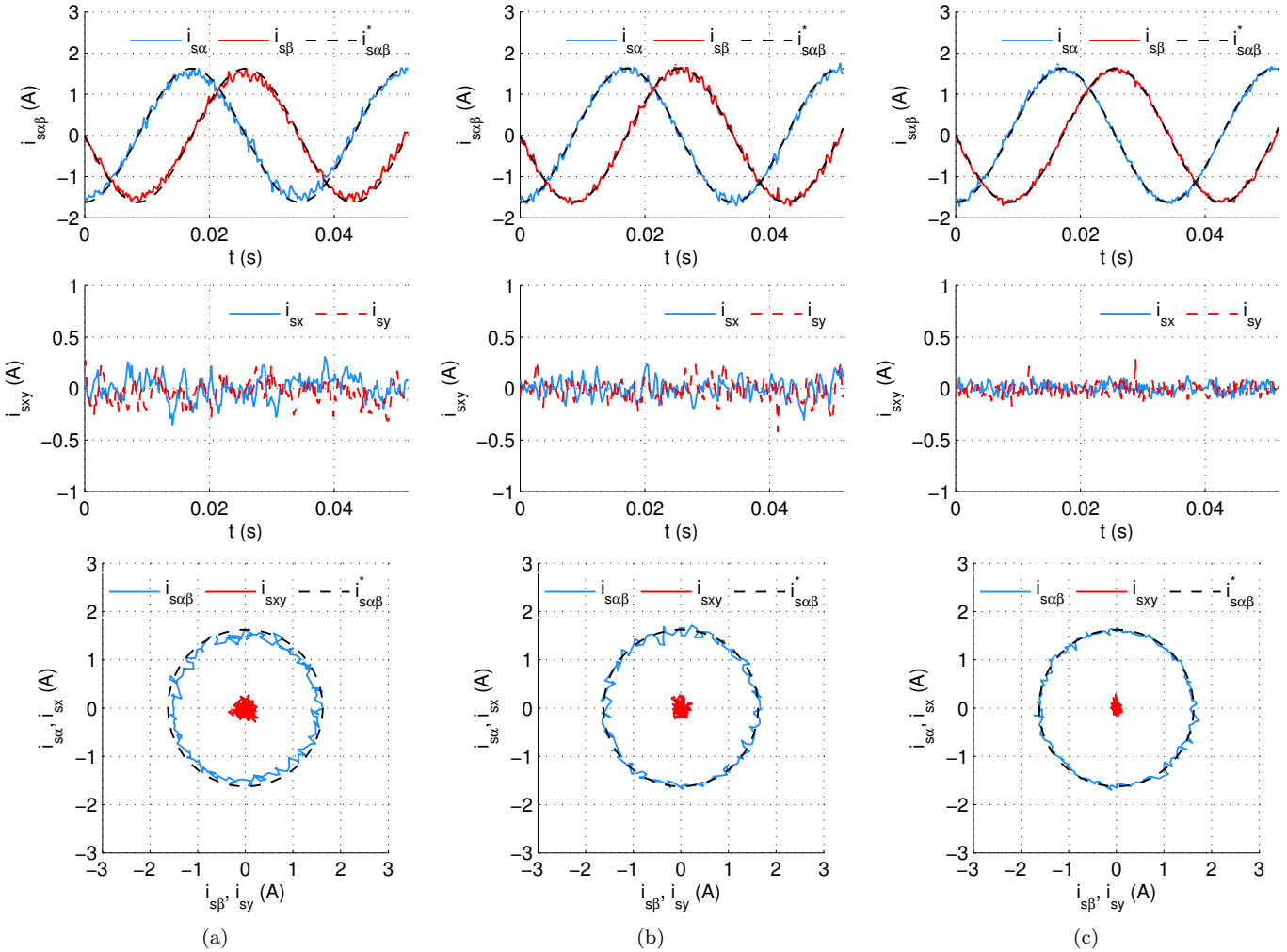

Figure 9: Experimental results obtained from the test rig for $A_{ref} = 1.62$ A and $f_e = 29$ Hz when it is applied the controller (a) FSMPC, (b) RLO and (c) FLO. Some graphics show the $\alpha - \beta$ stator currents (upper ones), $x - y$ stator currents (middle plots) and the same currents represented in circular trajectories (bottom draws).

are also presented in Fig. 9. The $\alpha - \beta - x - y$ current response of the system when $A_{ref} = 1.62$ A and $f_e = 29$ Hz is presented for the three considered controllers. It can be noted that using an observer produces a current response that better fits the reference than the conventional FSMPC method. Moreover, the current tracking is smoother for the full-order observer, as the ripple of the current signals is lower than in the reduced-order case. This is confirmed by the obtained RMS current tracking error values detailed in Table 2. For instance, the RMS error in the α current component is reduced by 28.12% and 39.36% for $f_e = 29$ Hz using RLO and FLO respectively. Similarly, the results for other operating points show that the reduction in e_{α}^{RMS} is higher for the full-order observer, with improvements of 31.60%, 35.04%, 45.46% and 49.63% for 19 Hz, 24 Hz, 34 Hz and 39 Hz respectively. Since $\alpha - \beta$ currents are directly related to the electromechanical energy conversion, the improved current tracking in the $\alpha - \beta$ plane reduces the torque ripple and enhances the dynamic performance. Also notice that the RMS current tracking error in the $x - y$ subspace is significantly reduced. The full-order observer achieves better e_{xy}^{RMS} values for all frequencies than the reduced-order one, obtaining an improvement in this figure of merit up to 56%. This is an interesting benefit of using observers because the lower RMS values of the $x - y$ currents do not affect the torque production (in distributed-winding machines), but it favours efficiency by reducing the IM copper losses.

The significant difference between both observers is principally due to the more accurate estimation of rotor currents that the full-order one produces, as evidenced by the prediction RMS error in the α current component values shown in Table 2. Although both observers improve this error with respect to the FSMPC, the FLO achieves a reduction that ranges from 35.04% to 45.72% with decreasing frequency, while the reduction with RLO ranges from 28.36% to 33.32% with increasing frequency.

Similarly, it can be stated from the results that the

switching changes per cycle N_c and the harmonic content THD are reduced when FSMPC is applied together with an observer, with the FLO control being the best option. Notice that the maximum improvement in N_c and THD is 26.81% and 10.85% for the reduced-order observer, and 34.15% and 30.27% for the full-order one. It is remarkable that the current tracking improvement obtained with the inclusion of observers is achieved with lower VSI switching frequency (i.e. lower values of N_c), which in turn implies that the VSI losses are also reduced.

From the computational cost perspective, one of the main drawbacks for the implementation of FSMPC in industry applications, the required computational load for implementing the rotor observer is negligible. The total computational cost of the control algorithm without rotor observer is estimated as about 32.4μs, while the incorporation of the reduced-order observer or the full-order one implies a total computational cost of 35.3μs and 35.7μs, respectively, with a sampling time of 67μs. It is important to indicate that both observers have similar computational costs, though the full-order one produces remarkable results in all aspects.

5. Conclusion

The area of model predictive control for multiphase electrical drives has experienced a substantial growth in the last years. Particularly, FSMPC strategy has been presented in the literature applied to the dual three-phase and five-phase drives. On the other hand, observers have been principally used in relation to IFOC, sensorless drives and for fault detection but, to the best of our knowledge, they have not been yet used together with FSMPC techniques. In this work, authors have proposed a current control scheme based on the FSMPC method incorporating a rotor current observer. The new estimation scheme has been assessed for a five-phase IM and has been demonstrated that it is possible to enhance the predictions including an observer without a considerable penalty in the computational burden of the controller. The experimental results show that, although the simple update and hold scheme used by most MPC practitioners in electrical applications produces acceptable results, the observer clearly outperforms the classic approach, presenting some advantages such as better current tracking performance, less harmonic content and less VSI gating commutations. Consequently, the use of observers together with MPC strategies generates torque with lower ripple and improves the overall efficiency by reducing both the copper and VSI losses. Moreover, two different observer structures have been designed and experimentally tested, a full-order observer and a reduced-order observer. It has been stated that the full-order one constitutes the best solution reducing the ripple in the currents trajectories, specially in the $x-y$ subspace, with a similar computational cost.

The proposed current control method can be applied to any n-phase induction machine, or even to conventional three-phase ones, just adjusting the predictive model and the observer equations to the new system. Consequently, these results encourage future research towards establishing the observer as a tool of choice for FSMPC to improve the behaviour in high-performance electrical drives.

Acknowledgments

The authors would like to thank the Junta de Andalucía and the Ministerio de Economía y Competitividad of the Spanish Government for their funding of this research under references P11-TEP-7555, DPI2013-44278-R, ENE2014-52536-C2-1-R.

References

Alireza Davari, S., Khaburi, D. A., Wang, F., Kennel, R. M., 2012. Using full order and reduced order observers for robust sensorless predictive torque control of induction motors. IEEE Transactions on Power Electronics 27 (7), 3424–3433.

Arahal, M. R., Barrero, F., Toral, S., Duran, M. J., Gregor, R., 2009. Multi-phase current control using finite-state model-predictive control. Control Engineering Practice 17 (5), 579–587.

Arahal, M. R., Castilla, M., Alvarez, J. D., Sánchez, J. A., 2013. Subharmonic content in finite-state model predictive current control of IM. In: IECON 2013-39th Annual Conference on IEEE Industrial Electronics Society. pp. 5866–5872.

Arashloo, R. S., Salehifar, M., Romeral, L., Sala, V., 2015. A robust predictive current controller for healthy and open-circuit faulty conditions of five-phase BLDC drives applicable for wind generators and electric vehicles. Energy Conversion and Management 92, 437–447.

Barrero, F., Duran, M. J., 2016. Recent advances in the design, modeling, and control of multiphase machines-Part I. IEEE Transactions on Industrial Electronics 63 (1), 449–458.

Bogado, B., Barrero, F., Arahal, M. R., Toral, S., Levi, E., 2013. Sensitivity to electrical parameter variations of predictive current control in multiphase drives. In: IECON 2013-39th Annual Conference on IEEE Industrial Electronics Society. pp. 5215–5220.

Chai, S., Wang, L., Rogers, E., 2013. Model predictive control of a permanent magnet synchronous motor with experimental validation. Control Engineering Practice 21 (11), 1584–1593.

Che, H. S., Levi, E., Jones, M., Hew, W.-P., Rahim, N. A., 2014. Current control methods for an asymmetrical six-phase induction motor drive. IEEE Transactions on Power Electronics 29 (1), 407–417.

Choi, D.-K., Lee, K.-B., 2015. Dynamic performance improvement of AC/DC converter using model predictive direct power control with finite control set. IEEE Transactions on Industrial Electronics 62 (2), 757–767.

Duran, M. J., Barrero, F., 2016. Recent advances in the design, modeling, and control of multiphase machines-Part II. IEEE Transactions on Industrial Electronics 63 (1), 459–468.

El Fadili, A., Giri, F., El Magri, A., Lajouad, R., Chaoui, F. Z., 2014. Adaptive control strategy with flux reference optimization for sensorless induction motors. Control Engineering Practice 26, 91–106.

Gopinath, B., 1971. On the control of linear multiple input-output systems. Bell System Technical Journal 50 (3), 1063–1081.

Guzman, H., Duran, M. J., Barrero, F., Zarri, L., Bogado, B., Gonzalez Prieto, I., Arahal, M. R., 2016. Comparative study of predictive and resonant controllers in fault-tolerant five-phase induction motor drives. IEEE Transactions on Industrial Electronics 63 (1), 606–617.

Hadiouche, D., Razik, H., Rezzoug, A., 2004. On the modeling and design of dual-stator windings to minimize circulating harmonic currents for VSI fed AC machines. IEEE Transactions on Industry Applications 40 (2), 506–515.

Holmes, D. G., Martin, D. A., Oct 1996. Implementation of a direct digital predictive current controller for single and three phase voltage source inverters. In: Industry Applications Conference, 1996. Thirty-First IAS Annual Meeting, IAS '96., Conference Record of the 1996 IEEE. Vol. 2. pp. 906–913 vol.2.

Holtz, J., Stadtfeld, S., 1983. A predictive controller for the stator current vector of AC machines fed from a switched voltage source. In: JIEE IPEC-Tokyo Conference. pp. 1665–1675.

Jansen, P. L., Lorenz, R. D., 1994. A physically insightful approach to the design and accuracy assessment of flux observers for field oriented induction machine drives. IEEE Transactions on Industry Applications 30 (1), 101–110.

Jones, M., Vukosavic, S. N., Dujic, D., Levi, E., 2009. A synchronous current control scheme for multiphase induction motor drives. IEEE Transactions on Energy Conversion 24 (4), 860–868.

Kautsky, J., Nichols, N. K., Van Dooren, P., 1985. Robust pole assignment in linear state feedback. International Journal of Control 41 (5), 1129–1155.

Levi, E., 2008. Multiphase electric machines for variable-speed applications. IEEE Transactions on Industrial Electronics 55 (5), 1893–1909.

Levi, E., Bojoi, R., Profumo, F., Toliyat, H. A., Williamson, S., 2007. Multiphase induction motor drives - a technology status review. IET Electric Power Applications 1 (4), 489–516.

Lim, C. S., Levi, E., Jones, M., Rahim, N. A., Hew, W. P., 2014. FCS-MPC-based current control of a five-phase induction motor and its comparison with PI-PWM control. IEEE Transactions on Industrial Electronics 61 (1), 149–163.

Lopez, M., Rodriguez, J., Silva, C., Rivera, M., 2015. Predictive torque control of a multidrive system fed by a dual indirect matrix converter. IEEE Transactions on Industrial Electronics 62 (5), 2731–2741.

Luenberger, D. G., 1971. An introduction to observers. IEEE Transactions on Automatic Control 16 (6), 596–602.

Martinez, J. L. R., Arashloo, R. S., Salehifar, M., Moreno, J. M., 2015. Predictive current control of outer-rotor five-phase BLDC generators applicable for off-shore wind power plants. Electric Power Systems Research 121, 260–269.

Merabet, A., Ouhrouche, M., Bui, R.-T., 2006. Nonlinear predictive control with disturbance observer for induction motor drive. In: 2006 IEEE International Symposium on Industrial Electronics. Vol. 1. pp. 86–91.

Riveros, J. A., Barrero, F., Levi, E., Durán, M. J., Toral, S., Jones, M., 2013. Variable-speed five-phase induction motor drive based on predictive torque control. IEEE Transactions on Industrial Electronics 60 (8), 2957–2968.

Riveros, J. A., Yepes, A., Barrero, F., Doval-Gandoy, J., Bogado, B., Lopez, O., Jones, M., Levi, E., 2012. Parameter identification of multiphase induction machines with distributed windings - Part 2: Time-domain techniques. IEEE Transactions on Energy Conversion 27 (4), 1067–1077.

Rodriguez, J., Kazmierkowski, M. P., Espinoza, J. R., Zanchetta, P., Abu-Rub, H., Young, H. A., Rojas, C. A., 2013. State of the art of finite control set model predictive control in power electronics. IEEE Transactions on Industrial Informatics 9 (2), 1003–1016.

Verghese, G. C., Sanders, S. R., 1988. Observers for flux estimation in induction machines. IEEE Transactions on Industrial Electronics 35 (1), 85–94.

Wang, F., Zhang, Z., Davari, A., Rodríguez, J., Kennel, R., 2014. An experimental assessment of finite-state predictive torque control for electrical drives by considering different online-optimization methods. Control Engineering Practice 31, 1–8.

Xia, C., Wang, M., Song, Z., Liu, T., 2012. Robust model predictive current control of three-phase voltage source PWM rectifier with online disturbance observation. IEEE Transactions on Industrial Informatics 8 (3), 459–471.

Xie, W., Wang, X., Wang, F., Xu, W., Kennel, R. M., Gerling, D., Lorenz, R. D., 2015. Finite-contro-set model predictive torque control with a deadbeat solution for PMSM drives. IEEE Transactions on Industrial Electronics 62 (9), 5402–5410.

Yepes, A. G., Malvar, J., Vidal, A., Lopez, O., Doval-Gandoy, J., 2015. Current harmonics compensation based on multiresonant control in synchronous frames for symmetrical n -phase machines. IEEE Transactions on Industrial Electronics 62 (5), 2708–2720.

Yepes, A. G., Riveros, J. A., Doval-Gandoy, J., Barrero, F., Lopez, O., Bogado, B., Jones, M., Levi, E., 2012. Parameter identification of multiphase induction machines with distributed windings - Part 1: Sinusoidal excitation methods. IEEE Transactions on Energy Conversion 27 (4), 1056–1066.

Zhang, Y., Yang, H., 2014. Model predictive torque control of induction motor drives with optimal duty cycle control. IEEE Transactions on Power Electronics 29 (12), 6593–6603.